Journal of Materials Chemistry C

PAPER

View Article Online
View Journal | View Issue

Cite this: J. Mater. Chem. C, 2017, 5, 5183

Polymorphism and mechanochromism of *N*-alkylated 1,4-dihydropyridine derivatives containing different electron-withdrawing end groups†

Yunxiang Lei, [a] Yibin Zhou, [a] Lebin Qian, [a] Yuxiang Wang, [b] Miaochang Liu, [a] Xiaobo Huang, *[a] Ge Wu, [c] Huayue Wu, *[a] Jinchang Ding [a] and Yixiang Cheng *[b]

Received 21st January 2017,
Accepted 8th May 2017

DOI: 10.1039/c7tc00362e

rsc.li/materials-c

Organic compounds exhibiting polymorphic and/or mechanochromic (MC) properties are promising for applications in multiple areas. However, the design strategy for such compounds is not very clear. Herein, several series of *N*-alkylated 1,4-dihydropyridine (DHP) derivatives incorporating different electron-withdrawing end groups were synthesized and compared. The electron-withdrawing groups were responsible for their polymorphic and MC properties. Additionally, a number of polymorphs of these DHP derivatives showed a decreasing trend as length of the alkyl chain increased, indicating that a longer alkyl chain was not conducive to formation of the polymorphs. Although differences in emissions of the polymorphs were mainly attributed to their different intermolecular interactions and molecular packing patterns, a subtle difference in the distances of their intermolecular interactions could also be a key factor in the formation of specific polymorphs. Different polymorphs of DHP derivatives could be interconverted by a simple recrystallization process with a specific solvent or through the application of pressure and vapor stimuli. Additionally, the MC properties of these DHP derivatives were ascribed to a phase transition between different crystalline states, instead of the more common transformation between crystalline and amorphous states.

Introduction

Solid-state organic compounds exhibiting switchable and variable fluorescence have recently attracted considerable interest owing to their potential applications in a wide range of fluorescent materials.[1] Two kinds of fluorescence characteristics, namely, mechanochromic (MC) and polymorphic properties, have been of particular interest in the development of these materials. MC compounds are a class of smart fluorescent materials with variable emission in response to pressure stimuli and their fluorescence can often be recovered by vapor and/or temperature stimuli based on the transformation between crystalline and amorphous states.[1b] Some compounds with polymorphic properties have a variety of crystal structures and exhibit distinctly different solid-state fluorescence,[2] and the interconversion of the emissions of these polymorphs can be ascribed to a transformation from one crystalline state to another. Recently, a number of compounds have been found to possess MC and polymorphic properties simultaneously,[3] however, the structural features that influence the presence of both MC and polymorphic properties and the design strategies for such compounds are not very clear; this remains a challenge and deserves further study.

4*H*-Pyran[4] and 1,4-dihydropyridine (DHP)[5] have been demonstrated to be good building units for the construction of donor–π–acceptor fluorescent materials. In particular, the introduction of an alkyl chain on the nitrogen atom is conducive to the formation of a distorted molecular conformation, which results in strong solid-state emission owing to restriction of intramolecular rotation.[6] Recently, we reported that some aggregation-induced-emission-active 4*H*-pyran and 1,4-dihydropyridine derivatives exhibited MC properties, solvent-induced solid-state emission changes, or acidochromic properties.[7] Unexpectedly, in the course of investigating the photophysical properties of these compounds, we found that an intermediate with a simple structure, 2-(1-ethyl-2,6-dimethylpyridin-4(1*H*)-ylidene)malononitrile (**MDHP-C$_2$**), showed both MC and polymorphic properties (Scheme 1). Considering that different electron-withdrawing end groups[7b,8]

[a] College of Chemistry and Materials Engineering, Wenzhou University, Wenzhou, 325035, P. R. China. E-mail: xiaobhuang@wzu.edu.cn, huayuewu@wzu.edu.cn
[b] School of Chemistry and Chemical Engineering, Nanjing University, Nanjing 210093, P. R. China. E-mail: yxcheng@nju.edu.cn
[c] School of Pharmacy, Wenzhou Medical University, Wenzhou 325035, P. R. China

† Electronic supplementary information (ESI) available: Experimental, characterization, crystal structures, fluorescence spectra, photophysical data, and other additional information. CCDC 1498114–1498127. For ESI and crystallographic data in CIF or other electronic format see DOI: 10.1039/c7tc00362e

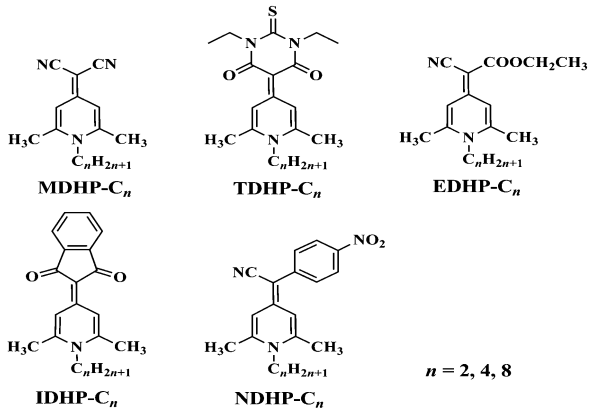

Scheme 1 Chemical structures of DHP derivatives.

and alkyl chain lengths[9] often played functional roles in modulating solid-state photophysical properties, we designed and synthesized several series of DHP derivatives with different alkyl chain lengths (ethyl, *n*-butyl, and *n*-octyl) on the nitrogen atom, namely **MDHP-C$_n$**, **TDHP-C$_n$**, **EDHP-C$_n$**, **IDHP-C$_n$**, and **NDHP-C$_n$** (n = 2, 4, 8), using malononitrile, 1,3-diethyl-2-thioxodihydropyrimidine-4,6(1*H*,5*H*)-dione, ethyl 2-cyanoacetate, 1*H*-indene-1,3(2*H*)-dione, and 2-(4-nitrophenyl)acetonitrile as electron-withdrawing end groups, respectively (Scheme 1). The electron-withdrawing end group had a significant impact on the solid-state fluorescence properties of these compounds. Compounds **MDHP-C$_n$**, **TDHP-C$_n$** (except **TDHP-C$_8$**), and **EDHP-C$_n$** all showed polymorphic and MC properties; however, **IDHP-C$_n$** and **NDHP-C$_n$** did not have these properties. Furthermore, the number of polymorphs of **MDHP-C$_n$** and **TDHP-C$_n$** showed a decreasing trend as the length of the alkyl chain increased. This difference in emissions of the polymorphs was mainly attributed to their different intermolecular interactions and molecular packing patterns, but interestingly, a subtle difference in the distances of the intermolecular interactions also played a crucial role in formation of the polymorphs, as revealed by crystallographic data. Different polymorphs of the DHP derivatives were interconverted by a simple recrystallization process with a specific solvent, grinding, or fuming. Additionally, X-ray diffraction (XRD) and differential scanning calorimetry (DSC) measurements indicated that the MC properties of these DHP derivatives were ascribed to the phase transition between different crystalline states, rather than the common transformation between crystalline and amorphous states.

Results and discussion

Synthesis and features of 4*H*-pyran and DHP derivatives

The synthetic route of the 4*H*-pyran and DHP derivatives is outlined in Scheme S1 (ESI†). Compounds **MP**,[6d,10] **MDHP-C$_n$**,[6d,7d,10,11] **EP**,[12] **EDHP-C$_8$**,[12] **IP**,[7a] and **IDHP-C$_n$**[7c] were synthesized according to previous literature procedures. The intermediates **TP** and **NP** were prepared from a Knoevenagel condensation of 2,6-dimethyl-4-pyrone with 1,3-diethyl-2-thioxodihydro-pyrimidine-4,6(1*H*,5*H*)-dione and 2-(4-nitrophenyl)acetonitrile, respectively. Reactions of **TP**, **EP**, and **NP** with corresponding aliphatic amines gave compounds **TDHP-C$_n$**, **EDHP-C$_2$**, **EDHP-C$_4$**, and **NDHP-C$_n$**, respectively, in good yields. Chemical structures of these compounds were characterized using nuclear magnetic resonance spectroscopy, element analysis, and mass spectrometry. Moreover, the structures of **MP**, **MDHP-C$_n$**, **TP**, **TDHP-C$_n$**, **IP**, **IDHP-C$_2$**, **EDHP-C$_4$**, and **NDHP-C$_2$** were further confirmed by single-crystal X-ray diffraction analysis (Fig. 1). The resulting compounds were easily soluble in common organic solvents such as tetrahydrofuran, toluene, ethyl acetate (EA), chloroform, acetonitrile, and acetone.

Fluorescence properties of 4*H*-pyran and DHP derivatives solids

Fluorescence spectra, excitation spectra, and fluorescence quantum yields (Φ_F) of the as-synthesized solids of various 4*H*-pyran derivatives were measured (Fig. S1, Tables S1 and S2, ESI†). The electron-withdrawing end groups had a significant impact on the solid-state fluorescence spectra of the 4*H*-pyran derivatives. Among these compounds, **MP** and **NP** showed the smallest and largest maximum emission wavelength (λ_{em}^{max}) at 481 and 599 nm with a low Φ_F value of 0.6 and 2.0%, respectively. The Φ_F values of **TP**, **EP**, and **IP** were 2.0, 31.4, and 20.4%, respectively. For the sake of discussion, herein, the solids of all the DHP derivatives obtained by a recrystallization of their as-synthesized solids using a mixed solvent of *n*-hexane and $CHCl_3$ (30 : 1, v : v) were regarded as their original samples. Fluorescence spectra of the original samples of **MDHP-C$_n$**, **TDHP-C$_n$**, and **EDHP-C$_n$** showed an obvious blue shift compared with those of the corresponding 4*H*-pyran derivatives, whereas the original samples of **IDHP-C$_n$** and **NDHP-C$_n$** exhibited an obvious red shift (Fig. S2, ESI†). Although the introduction of an *N*-alkyl chain is beneficial for enhancing the degree of distortion of a molecular structure, and promoting a blue shift in the fluorescence spectra,[7c] emissions of the solid materials are also closely related to their molecular packing patterns.

Polymorphic and MC properties of DHP derivatives

The synthetic route of 4*H*-pyran and DHP derivatives is outlined. The original sample of **MDHP-C$_2$** emitted strong blue fluorescence at 461 nm with a Φ_F value of 48.8% (Fig. 2, 3 and Table S1, ESI†). Moreover, two different types of single-crystal structures of **MDHP-C$_2$**, namely **MDHP-C$_2$-*c*** and **MDHP-C$_2$-*l***, were cultured by slow diffusion of *n*-hexane into the $CHCl_3$ solution of the original sample and recrystallized using acetonitrile as a solvent, respectively. **MDHP-C$_2$-*c*** emitted cyan fluorescence at 470 nm with a Φ_F value of 79.7%, whereas, lawn green-emitting **MDHP-C$_2$-*l*** exhibited a redder emission at 489 nm with a lower quantum yield of 57.2%. According to their XRD measurements, diffraction curves of the original samples, **MDHP-C$_2$-*c***, and **MDHP-C$_2$-*l*** all revealed sharp and intense reflection peaks (Fig. 4), which are characteristic properties of microcrystalline structures. These results suggested that **MDHP-C$_2$** should be a polycrystalline fluorophore. The difference in emissions between different crystal structures could be mainly attributed to their different intermolecular interactions and molecular packing patterns,[2d] which is discussed in the crystal structure analysis section below. The three crystal polymorphs could be interconverted by a simple

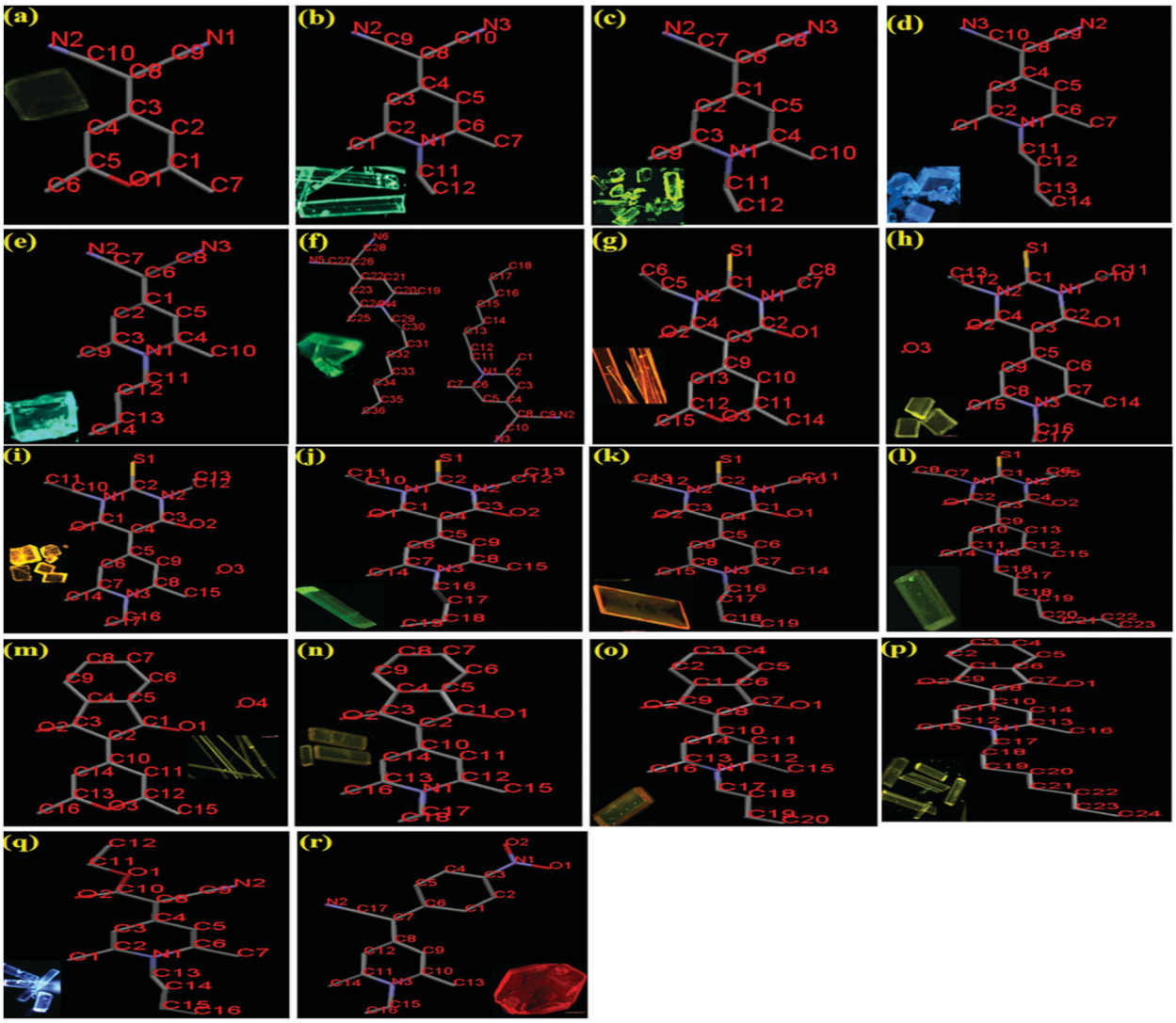

Fig. 1 Single-crystal structures of some 4*H*-pyran and DHP derivatives: (a) **MP**; (b) **MDHP-C_2-*c***; (c) **MDHP-C_2-*l***; (d) **MDHP-C_4-*sb***; (e) **MDHP-C_4-*lc***; (f) **MDHP-C_8-*c***; (g) **TP**; (h) **TDHP-C_2-*ly***; (i) **TDHP-C_2-*o***; (j) **TDHP-C_4-*g***; (k) **TDHP-C_4-*o***; (l) **TDHP-C_8**; (m) **IP**; (n) **IDHP-C_2**; (o) **IDHP-C_4**; (p) **IDHP-C_8**; (q) **EDHP-C_4**; and (r) **NDHP-C_2**. Hydrogen atoms are omitted for clarity. Inset: Fluorescence image of the corresponding single crystal taken under 365 nm UV light.

recrystallization process with an appropriate solvent (Fig. 2). A fluorescence color change from blue to yellow-green ($\Delta\lambda_{MC}$ = 41 nm, Table S1, ESI†) was clearly observed after the original crystalline sample of **MDHP-C_2** was ground with a pestle in a mortar, suggesting that the original sample exhibited distinct MC properties. If the ground sample was exposed to EA vapor, its fluorescence returned to that of the original sample, suggesting a reversible MC behavior. It is noteworthy that the reflection peaks in the XRD curve of the ground sample were still sharp and intense except that several peaks (2θ = 17.4°, 24.3°, and 26.9°) showed obvious changes (Fig. 4), indicating the ground sample should also have a crystalline structure. Furthermore, according to the DSC experiments, no cold-crystallization transition was detected before the isotropic melt transition of the ground sample (Fig. S3, ESI†), indicating that the ground sample should not be amorphous but crystalline. These results indicated that the MC properties could be ascribed to a phase transition between different crystalline states,[2h,3d] rather than the common transformation between crystalline and amorphous states. Moreover, we investigated the stimulus response behaviors of **MDHP-C_2-*c*** and **MDHP-C_2-*l*** upon grinding. Interestingly, by grinding these two types of single crystals with a gentle pressure, a blue-emitting solid (λ_{em} = 459 nm, Φ_F = 51.3%) in line with the original sample was obtained, whereas a yellow-green-emitting solid (λ_{em} = 502 nm, Φ_F = 40.3%) was obtained using a hard pressure, same as the ground sample obtained from the original sample, indicating **MDHP-C_2-*c*** and **MDHP-C_2-*l*** displayed multicolored MC behavior. These results demonstrated that the emissions of **MDHP-C_2** could be switched between four colors in the solid state by a transformation between four crystalline forms.

MDHP-C_4 had three different crystal polymorphs (Fig. 5, Fig. S4, S5 and Table S1, ESI†), including the original sample

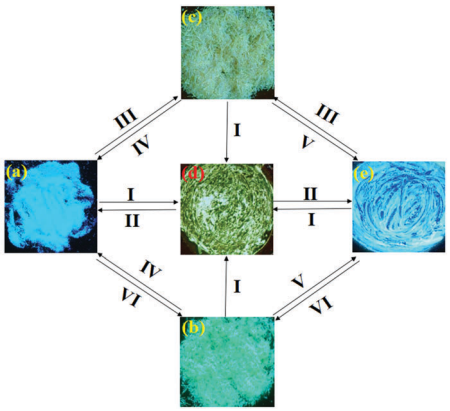

Fig. 2 Fluorescence images of **MDHP-C$_2$** solid samples taken under UV irradiation at 365 nm: (a) original sample; (b) **MDHP-C$_2$-*c*** sample; (c) **MDHP-C$_2$-*l*** sample; (d) strongly ground sample; and (e) gently ground sample. Conditions: (I) hard grinding; (II) fuming with EA vapor; (III) a recrystallization process using acetonitrile as a solvent; (IV) a recrystallization process using *n*-hexane/$CHCl_3$ (30 : 1, v : v); (V) gentle grinding; and (VI) slow diffusion of *n*-hexane/$CHCl_3$ (6 : 1, v : v).

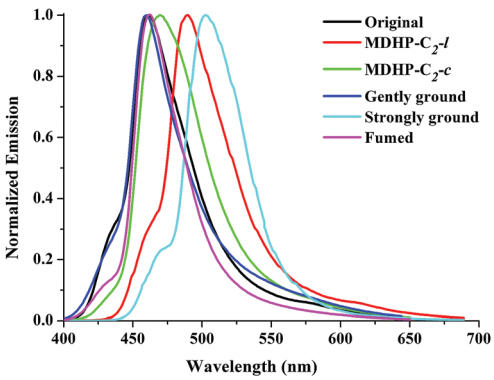

Fig. 3 Normalized emission spectra of **MDHP-C$_2$** solid samples under different conditions.

(λ_{ex}^{max} = 447 nm, Φ_F = 30.1%), **MDHP-C$_4$-*sb*** (λ_{ex}^{max} = 456 nm, Φ_F = 38.9%), and **MDHP-C$_4$-*lc*** (λ_{ex}^{max} = 466 nm, Φ_F = 18.1%). Upon slow diffusion of *n*-hexane/$CHCl_3$ (6 : 1, v : v), single crystals of **MDHP-C$_4$-*sb*** with a sky-blue emission were formed, whereas single crystals of **MDHP-C$_4$-*lc*** with a light cyan emission were obtained by a recrystallization with acetonitrile (Fig. 5). In contrast to **MDHP-C$_2$**, after being ground, the original blue-emitting sample of **MDHP-C$_4$** did not show an obvious fluorescence color change, whereas **MDHP-C$_4$-*sb*** and **MDHP-C$_4$-*lc*** displayed a blue shift of 9 and 19 nm and returned to their original crystal samples (Fig. S3, ESI†), respectively, exhibiting MC properties. In comparison to **MDHP-C$_2$** and **MDHP-C$_4$**, only two types of crystals for **MDHP-C$_8$**, namely the original sample and cyan-emitting **MDHP-C$_8$-*c***, were obtained (Fig. S6–S8, ESI†), indicating a longer alkyl chain was unfavorable for the formation of polymorphic crystals. Moreover, the grinding of **MDHP-C$_8$-*c*** altered its emission from cyan to blue and the ground sample was almost identical to the original sample.

Similarly, **TDHP-C$_2$** and **TDHP-C$_4$** also exhibited polymorphic and MC properties, and showed three and five individual

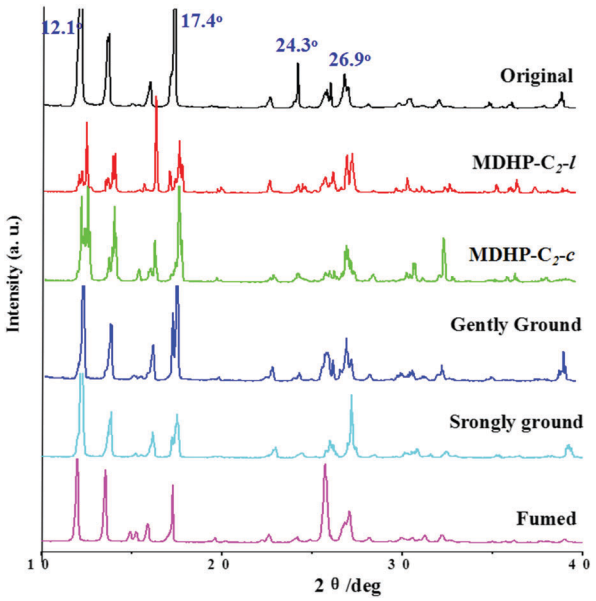

Fig. 4 XRD curves of **MDHP-C$_2$** solid samples under different conditions. The peaks of the original sample at 2θ = 12.1° and 17.4° are truncated to better show the fine structures.

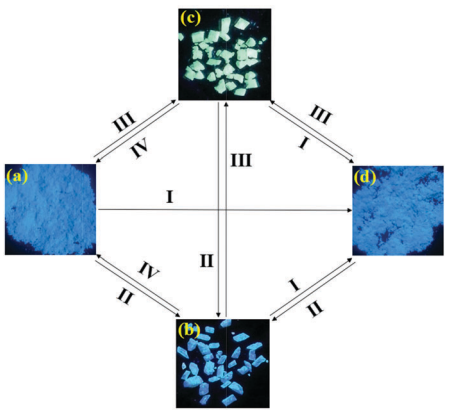

Fig. 5 Fluorescence images of **MDHP-C$_4$** solid samples taken under UV irradiation at 365 nm: (a) original sample; (b) **MDHP-C$_4$-*sb*** sample; (c) **MDHP-C$_4$-*lc*** sample; and (d) ground sample. Conditions: (I) grinding; (II) slow diffusion of *n*-hexane/$CHCl_3$ (6 : 1, v : v); (III) a recrystallization process using CH_3CN as a solvent; and (IV) a recrystallization process using *n*-hexane/$CHCl_3$ (30 : 1, v : v).

emission colors in their crystalline states, respectively. The original crystalline sample of **TDHP-C$_2$** exhibited weak pale-yellow fluorescence with a Φ_F value of 7.5% (Fig. 6 and Table S1, ESI†). The two crystalline polymorphs **TDHP-C$_2$-*ly*** and **TDHP-C$_2$-*o*** obtained from a slow diffusion of *n*-hexane/$CHCl_3$ (6 : 1, v : v) and a slow evaporation of $CHCl_3$/EA (1 : 6, v : v) displayed light yellow (λ_{em} = 458, 596 nm) and orange (λ_{em} = 456, 597 nm) fluorescence, respectively, with quantum yields of 12.2% and 10.7%. After grinding, the ground samples of these two crystals exhibited similar XRD curves and fluorescence spectra as those of the original samples (Fig. S9 and S10, ESI†). For **TDHP-C$_4$** (Fig. 7, Fig. S11 and S12, ESI†), interestingly, two kinds of original samples,

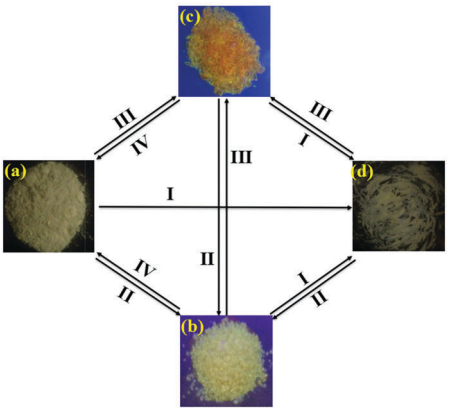

Fig. 6 Fluorescence images of **TDHP-C$_2$** solid samples taken under UV irradiation at 365 nm: (a) original sample; (b) **TDHP-C$_2$-*ly***; (c) **TDHP-C$_2$-*o***; and (d) ground sample. Conditions: (I) grinding; (II) slow diffusion of *n*-hexane/$CHCl_3$ (6 : 1, v : v); (III) slow evaporation of $CHCl_3$/EA (1 : 6, v : v); and (IV) a recrystallization process using *n*-hexane/$CHCl_3$ (30 : 1, v : v).

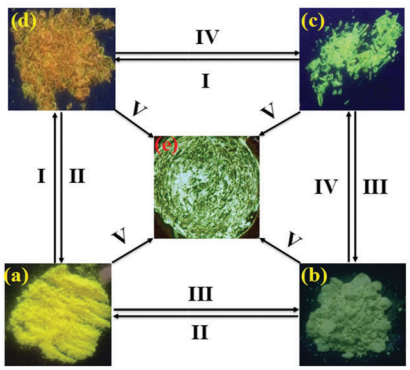

Fig. 7 Fluorescence images of **TDHP-C$_4$** solid samples taken under UV irradiation at 365 nm: (a) **TDHP-C$_4$-OSA**; (b) **TDHP-C$_4$-OSB**; (c) **TDHP-C$_4$-*g***; (d) **TDHP-C$_4$-*o***; and (e) ground sample. Conditions: (I) slow evaporation of $CHCl_3$/EA (1 : 6, v : v); (II) a recrystallization process using *n*-hexane/$CHCl_3$ (30 : 1, v : v); (III) a recrystallization process using *n*-hexane/$CHCl_3$ (60 : 1, v : v); (IV) slow diffusion of *n*-hexane/$CHCl_3$ (6 : 1, v : v); and (V) grinding with a pestle in a mortar.

namely yellow-emitting solids **TDHP-C$_4$-OSA** (λ_{em} = 463, 542 nm, Φ_F = 14.7%) and dark sea-green-emitting solids **TDHP-C$_4$-OSB** (λ_{em} = 456, 533 nm, Φ_F = 10.9%), were obtained by recrystallization using *n*-hexane/$CHCl_3$ with different volume ratios (v : v = 30 : 1 for the former and v : v = 60 : 1 for the latter). There was a slow precipitation process for the former and a fast precipitation process for the latter, indicating that these different recrystallization methods led to different morphologies.[3e] Furthermore, the green-emitting single crystal **TDHP-C$_4$-*g*** (λ_{em} = 508 nm, Φ_F = 15.9%) was generated by slow diffusion of *n*-hexane/$CHCl_3$ (6 : 1, v : v) and another orange-emitting single crystal **TDHP-C$_4$-*o*** (λ_{em} = 543, 581 nm, Φ_F = 20.1%) was obtained by slow evaporation of $CHCl_3$/EA (1 : 6, v : v). After grinding, the two original samples and the two crystalline polymorphs all converted to their solids with a yellow-green emission (λ_{em} = 467, 538 nm, Φ_F = 11.2%). For **TDHP-C$_8$**, only a green-emitting crystal sample was obtained, and the fluorescent color and XRD curves did not show a clear change after grinding, suggesting it was MC inactive (Fig. S13 and S14, ESI†). Generally, **TDHP-C$_2$-*ly***, **TDHP-C$_4$-*g***, and **TDHP-C$_4$-OSB**, which exhibit blue-shifted emissions, should have higher fluorescence efficiencies than **TDHP-C$_2$-*o***, **TDHP-C$_4$-*o***, and **TDHP-C$_4$-OSA**, which exhibit red-shifted emissions, owing to a stronger intermolecular interaction (see below); however, the opposite results were observed (Table S1, ESI†). To explain this abnormal phenomenon, we investigated time-resolved fluorescence decay parameters of these TDHP derivatives in the solid state (Table S3, ESI†). As shown in Table S3 (ESI†), compared with **TDHP-C$_2$-*o*** and **TDHP-C$_4$-OSA**, **TDHP-C$_2$-*ly*** and **TDHP-C$_4$-OSB** had a smaller radiative rate constant (k_f) and a larger non-radiative rate constant (k_{nr}), respectively. Additionally, although the k_f value of **TDHP-C$_4$-*g*** was 5.4 × 10^7 s^{-1} and larger than that of **TDHP-C$_4$-*o*** (3.7 × 10^7 s^{-1}), the k_{nr} value (2.9 × 10^8 s^{-1}) of **TDHP-C$_4$-*g*** was nearly two times higher than that of **TDHP-C$_4$-*o*** (1.5 × 10^8 s^{-1}). Herein, the larger non-radiative decay resulted in fluorescence quenching, which might account for the lower fluorescence efficiencies of the TDHP derivatives with bluer emissions.[3d]

After grinding, changes in the fluorescence color of the original samples of **EDHP-C$_n$** were clearly observed (Fig. S15, ESI†). Interestingly, although there was only a 4 and 5 nm red shift in the maximum emission wavelengths for the original samples of **EDHP-C$_2$** and **EDHP-C$_4$**, respectively, after they were ground (Fig. S16 and Table S2, ESI†), their emission profiles displayed obvious changes, namely, the intensity of the peak at approximately 424 nm showed a remarkable decrease, which could explain changes in the fluorescence color. Although grinding led to changes of some reflection peaks in the XRD curves of **EDHP-C$_n$** solids (Fig. S17, ESI†), their crystalline structures were still maintained. Meanwhile, there was no cold-crystallization phenomenon observed upon heating the ground samples according to their DSC curves (Fig. S18, ESI†). These results indicated that **EDHP-C$_n$** solids have two kinds of crystal polymorphs and their MC properties were caused by a crystal-to-crystal transformation. After the ground samples were fumed with EA vapor, their emission colors and fluorescent spectra were reversed to those of the emissive original samples. For yellow-emitting **IDHP-C$_n$** (Fig. S19–S21, ESI†) and red-emitting **NDHP-C$_n$** (Fig. S22–S24, ESI†), only one kind of crystal form was obtained and grinding had no obvious influence on the fluorescence spectra and XRD curves of their solid samples, and thus could not change their fluorescence colors. Especially, solid-state **NDHP-C$_4$** did not emit fluorescence but the reason remained unclear because its single crystal could not be obtained.

Crystal structures of DHP derivatives

To gain a better understanding of the underlying reason for the photophysical behaviors of the DHP derivatives in different aggregated states, crystal structure analysis was performed to investigate their molecular conformations and packing patterns in their crystalline states. For the two crystal polymorphs of **MDHP-C$_2$**, unit cells of **MDHP-C$_2$-*c*** and **MDHP-C$_2$-*l*** were both triclinic with a $P\bar{1}$ space group (Table S4, ESI†). In contrast to that of **MP**, which had a planar structure, these two polymorphs adopted a twisted conformation in which the torsion angles

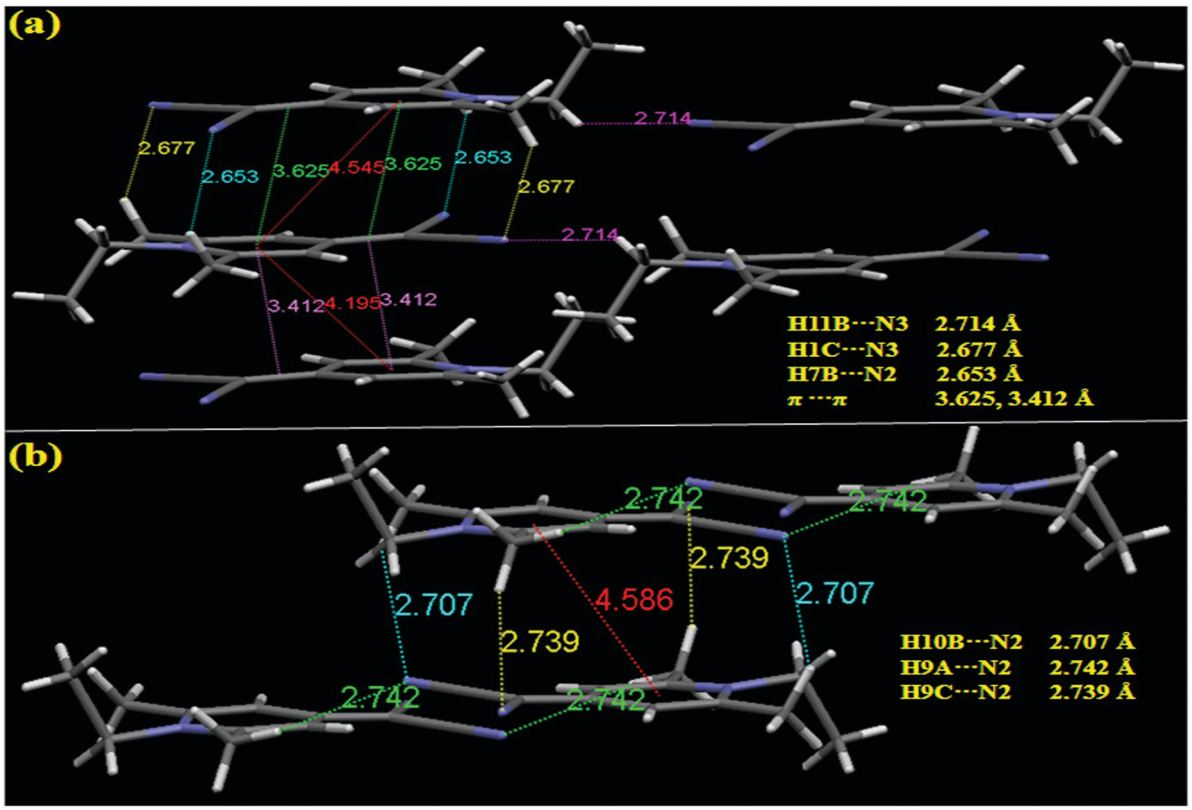

Fig. 8 Schematic diagram of the intermolecular interactions in the crystals of **MDHP-C_2-*c*** (a) and **MDHP-C_2-*l*** (b).

between the *N*-ethyl group and the DHP unit were 80.23° and 80.01°, respectively. Molecules of the crystals of **MDHP-C_2-*c*** were stabilized by π–π stacking interactions and C–H···N bonds (Fig. 8). The distances between the DHP unit and the olefinic double bond in the upper and lower molecules were measured to be 3.625 and 3.412 Å, respectively, indicating the existence of π–π stacking. Furthermore, two types of aliphatic C–H···N bonds (2.677 and 2.653 Å) between a H atom of the ethyl moiety and the N atom in the cyano group were formed in the same column, and another C–H···N bond (2.714 Å) restricted the adjacent molecules between the two columns. There was no π–π stacking in the crystal of **MDHP-C_2-*l*** and only three kinds of aliphatic C–H···N bonds (2.707, 2.739, and 2.742 Å) restricted the adjacent molecules. These results indicated that crystals of **MDHP-C_2-*c*** had stronger intermolecular interactions than crystals of **MDHP-C_2-*l***. We further investigated the molecular packing modes of **MDHP-C_2-*c*** and **MDHP-C_2-*l*** in these crystals. As shown in Fig. 9, although these two crystal polymorphs both adopted a head-to-tail packing pattern, their packing arrangements showed distinct differences. The molecules of **MDHP-C_2-*l*** and **MDHP-C_2-*c*** along the *b*-axis were arranged in a single chain and ribbons, respectively. Furthermore, for **MDHP-C_2-*l***, the overlap between two pairs of head-to-tail molecules along the *c*-axis was obviously poorer compared with that of **MDHP-C_2-*c***.

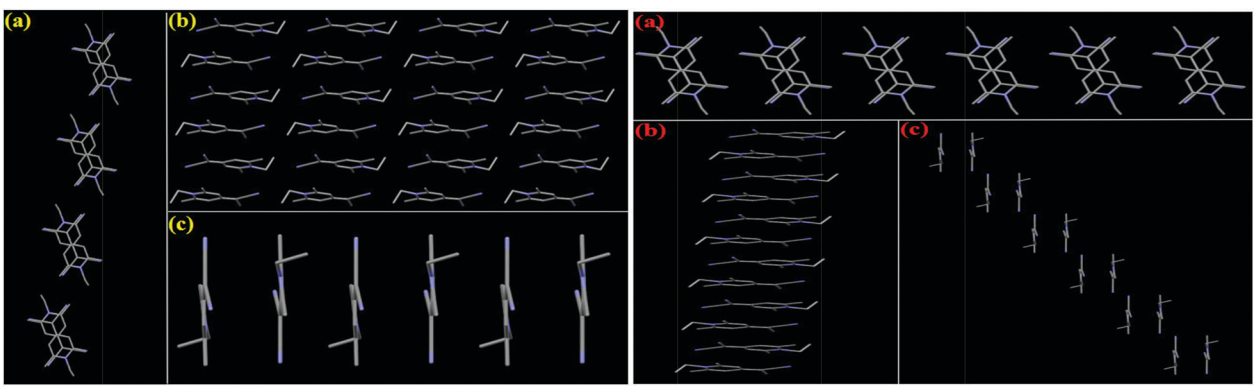

Fig. 9 Packing patterns in the crystal of **MDHP-C_2-*c*** (left) and **MDHP-C_2-*l*** (right): (a) viewed along the *a*-axis; (b) viewed along the *b*-axis; (c) viewed along the *c*-axis. The hydrogen atoms have been omitted for clarity.

These results indicated that packings of **MDHP-C_2-*c*** in the crystals were more compact compared to those of **MDHP-C_2-*l***.

Stronger intermolecular interactions and closer molecular packing should inhibit the molecules of **MDHP-C_2-*c*** from having some sort of motion and thus lead to a blue shifted emission and higher Φ_F value compared to those of **MDHP-C_2-*l***.[3j] These results also indicated that the different intermolecular interactions and molecular packing arrangements were the main reasons for the observed polymorphism of **MDHP-C_2**. Because of the parallel stacking patterns in these two crystals, it was relatively easy for the crystal structure to change into other crystal forms upon gentle or hard grinding, and thus result in MC properties. However, their crystalline structures were not easily destroyed by grinding because of strong intermolecular interactions. Therefore, their MC properties could be ascribed to the transformations between different crystalline states. Although the original/gently ground sample emitting blue fluorescence was obtained by recrystallization using a mixed solvent of *n*-hexane and $CHCl_3$, unfortunately, only the single crystal of cyan-emitting **MDHP-C_2-*c***, instead of the original/gently ground sample, was obtained by slow diffusion of *n*-hexane/$CHCl_3$, even using a variety of different volume ratios. Therefore, we were unable to investigate the transformation between different crystalline states.

In the case of the crystal polymorphs of **TDHP-C_2**, the unit cell of **TDHP-C_2-*ly*** was monoclinic with a $P2(1)/n$ space group and that of **TDHP-C_2-*o*** was monoclinic with a $P2(1)/n$ space group (Table S5, ESI†). **TDHP-C_2-*ly*** and **TDHP-C_2-*o*** both adopted a head-to-tail packing pattern in pairs, in which the DHP ring stacked with the 2-thioxodihydropyrimidine ring in a face-to-face manner, and the dihedral angle between two pairs of molecules was 85.18° and 85.29°, respectively. These two crystal polymorphs were stabilized by weak π–π stacking interactions (3.849 Å for **TDHP-C_2-*ly*** and 3.857 Å for **TDHP-C_2-*o***), aliphatic C–H···S bonds (2.975 Å for **TDHP-C_2-*ly*** and 2.984 Å for **TDHP-C_2-*o***), and aliphatic C–H···π bonds (3.275–3.698 Å for **TDHP-C_2-*ly*** and 3.281–3.756 Å for **TDHP-C_2-*o***) from adjacent molecules, whereas the interaction distances of **TDHP-C_2-*ly*** were obviously shorter than those of **TDHP-C_2-*o*** (Fig. 10). Moreover, as depicted in Fig. 11, although they exhibited the same packing arrangement along the *a*-axis, the packing of **TDHP-C_2-*o*** along the *b*-axis and the *c*-axis was looser compared with that of **TDHP-C_2-*ly***, which should be the reason that the emission of the former showed obvious red shift compared to that of the latter.

The crystals of **MDHP-C_4-*sb*** and **MDHP-C_4-*lc*** were mainly stabilized by C–H···N bonds, C–H···π bonds, and π–π stacking interactions between the DHP rings (Fig. S25, ESI†). Interestingly, these two polymorphs showed the same molecular packing pattern in the crystals (Fig. S26, ESI†). There was a subtle difference in the distances of the intermolecular interactions of **MDHP-C_4-*sb***, which were all shorter than the corresponding distances of **MDHP-C_4-*lc*** (Fig. S25, ESI†), indicating more intense intermolecular forces between the molecules in the former crystals. As a result, the molecules in the crystal lattice of **MDHP-C_4-*sb*** accumulated more closely and thus had a smaller volume and a larger density (655.05 $Å^3$ and 1.152 Mg m^{-3}) compared to those of **MDHP-C_4-*lc*** (680.9 $Å^3$ and 1.109 Mg m^{-3}) (Table S4, ESI†). A similar phenomenon was observed in the two polymorphs of **TDHP-C_4**, namely **TDHP-C_4-*g*** and **TDHP-C_4-*o***, (Fig. S27, S28 and Table S4, ESI†). Based on these results, a minor difference in the distances of the intermolecular interactions can also play a crucial role in formation of the polymorphs.

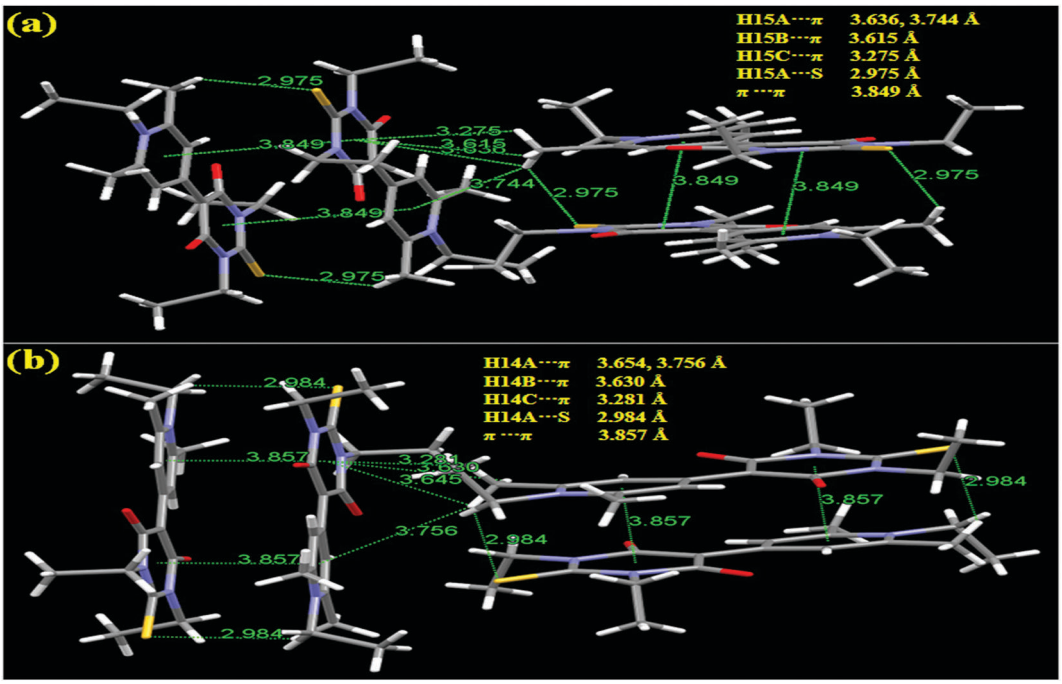

Fig. 10 Schematic diagram of the intermolecular interactions in the crystals of **TDHP-C_2-*ly*** (a) and **TDHP-C_2-*o*** (b).

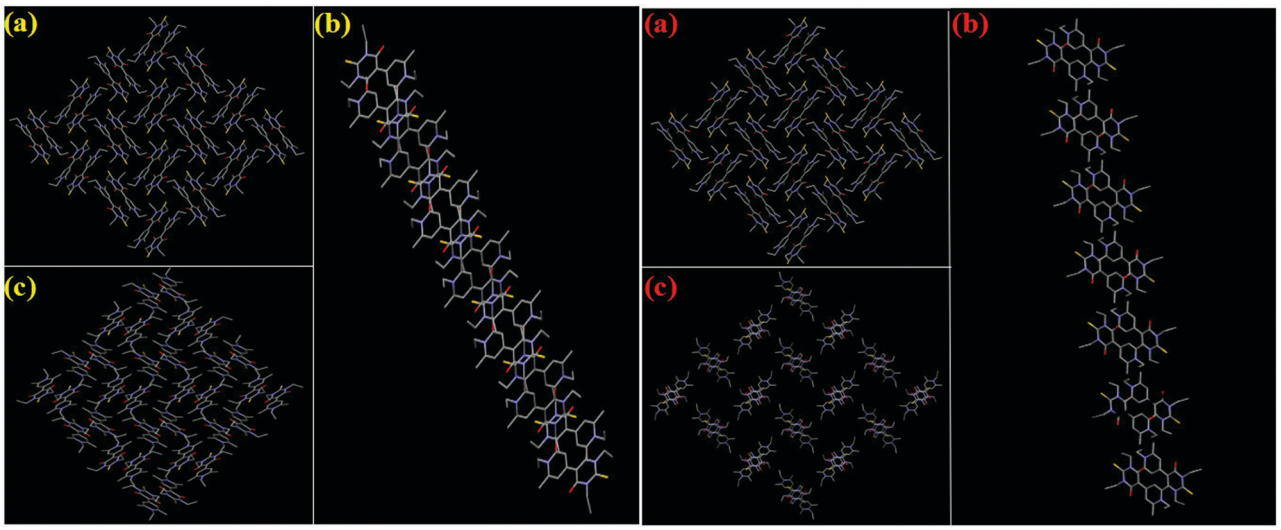

Fig. 11 Packing patterns in the crystals of **TDHP-C$_2$-*ly*** (left) and **TDHP-C$_2$-*o*** (right): (a) viewed along the *a*-axis; (b) viewed along the *b*-axis; and (c) viewed along the *c*-axis. The hydrogen atoms have been omitted for clarity.

It should be noted that the number of polymorphs of **TDHP-C$_n$** and **MDHP-C$_n$** generally decreased as the length of the alkyl chain increased. Only two types of crystals were obtained for **MDHP-C$_8$** and one type for **TDHP-C$_8$**. **MDHP-C$_8$-*c***; they belong to the monoclinic crystal system and have a *Pc* space group (Table S4, ESI†). There were six kinds of intermolecular C–H···N bonds (2.516–2.735 Å) and five kinds of C–H···π bonds (2.840–3.494 Å) in the crystals (Fig. S29, ESI†). Compared with the polymorphs of **MDHP-C$_2$** and **MDHP-C$_4$**, the regularity and rigidity of the crystal alignment of **MDHP-C$_8$-*c*** was clearly poorer as a result of introducing the long *n*-octyl chain, indicating that the *n*-octyl group was not advantageous to the varied balances of weak intermolecular interactions between molecules in the solid state and thereby the formation of different polymorphs. Additionally, **MDHP-C$_8$-*c*** had a larger volume (1664.7 Å^3) and a smaller density (1.131 Mg m^{-3}) in its crystal lattice (Table S5, ESI†). For **TDHP-C$_8$**, two kinds of C–H···O bonds (2.519 and 2.520 Å) and four kinds of π···π interactions (3.351–3.723 Å) stabilized its crystal structure (Fig. S30, ESI†). Interestingly, **TDHP-C$_8$**, which was quite different from the other **MDHP** and **TDHP** derivatives, did not show MC properties, which might be attributed to its one kind of crystal form and thus the transformation from one crystalline state to another crystalline state could not be implemented.

As for **EDHP-C$_n$**, we just only obtained the blue-emitting single crystal of **EDHP-C$_4$** from a slow diffusion of *n*-hexane/$CHCl_3$ (6 : 1, v : v). As revealed by the crystal structure of **EDHP-*C*$_4$** (Fig. S31, ESI†), molecules in the same layer were restricted by one kind of aliphatic C–H···O bond (2.336 Å), and those in the upper and lower layers were stabilized by one kind of π–π stacking interaction (3.513 Å), one kind of aliphatic C–H···O bond (2.669 Å), and one kind of van der Waals force between aliphatic hydrogen atoms in the *N*-butyl chains (with a distance of 2.383 Å). As a result, the molecules of **EDHP-C$_4$** adopted a stair-like stacking mode, which allowed it to be easily changed into another crystal mode upon grinding.

In the case of **IDHP-C$_n$**, a yellow-emitting single crystal of **IDHP-C$_2$** was obtained from slow diffusion of *n*-hexane/$CHCl_3$ (6 : 1, v : v), and the crystal data of **IDHP-C$_4$** and **IDHP-C$_8$** was obtained from our previous report.[7c] The molecules of **IDHP-C$_2$**, **IDHP-C$_4$**, and **IDHP-C$_8$** in their crystals were stabilized by one kind of π–π stacking interaction, two kinds of C–H···π bonds, and two, six, and four kinds of C–H···O bonds between adjacent molecules, respectively (Fig. S32–S34, ESI†). **IDHP-C$_2$** and **IDHP-C$_4$** both adopted a head-to-tail packing pattern in pairs and packed in a tight zigzag shape. Herein, because of the strong intermolecular interactions and tight packing mode, the crystal structures of these compounds were not easy to change upon grinding, which was also confirmed by results from the XRD experiments before and after grinding (Fig. S21, ESI†). Although **IDHP-C$_8$** packed in a reverse lamellar structure, strong intermolecular interactions still guaranteed the stability of its crystal structure, avoiding being affected by external pressure (Fig. S34, ESI†).

The unit cell of **NDHP-C$_2$** was monoclinic with a *P*2(1)/*c* space group (Table S6, ESI†). As revealed by the crystal structure of **NDHP-C$_2$** (Fig. S35, ESI†), the molecule exhibited a twisted conformation due to introduction of steric hindrance from a large 4-nitrophenyl group, and the dihedral angle between the DHP ring and benzene ring was 35.29°. Interestingly, in comparison with the other DHP derivatives containing an *N*-ethyl group, the original sample of **NDHP-C$_2$** had a larger emission wavelength (640 nm) and emitted red fluorescence, which was ascribed to the stronger electron withdrawing ability and larger conjugated system of the 4-nitrophenyl group. The distance between the two phenyl rings in the upper and lower layers was measured to be 4.066 Å, which indicated the absence of π–π stacking. The crystal structure was stabilized by three kinds of C–H···N bonds (2.689, 2.703, and 2.705 Å), two kinds of C–H···π bonds (2.793 and 2.811 Å), and one kind of C–H···O bond (2.935 Å) from adjacent molecules, adopting an offset face-to-face arrangement in the upper and lower layers and a head-to-tail arrangement in the same layer. Similar to **IDHP-C$_8$**, strong interactions between molecules ensured that the crystal structure of this compound was not damaged by grinding.

Conclusions

Several series of DHP derivatives were synthesized to investigate the influence of different electron-withdrawing end groups and alkyl chain lengths on their polymorphic and MC properties. Most of **MDHP-C$_n$**, **TDHP-C$_n$**, and **EDHP-C$_n$** had a variety of crystals emitting different fluorescence and showed obvious MC properties; however, compounds **IDHP-C$_n$** and **NDHP-C$_n$** only had one type of crystal and were MC inactive. These results revealed that the electron-withdrawing end group played a vital role in the generation of MC and polymorphic properties of the DHP derivatives. A possible reason is that the electron-withdrawing end group, with different steric and electronic effects, had a significant influence on the generation of appropriate intermolecular interactions between molecules and proper molecular packing patterns in the crystals which could result in formation of specific polymorph and MC properties. Furthermore, the alkyl chain length had an obvious effect on the number of crystal polymorphs for **MDHP-C$_n$** and **TDHP-C$_n$**; specifically, an increase in the alkyl chain length decreased the number of crystal polymorphs in a trend. Single crystal analysis showed that the difference in emissions of the polymorphs of the DHP derivatives mainly originated from their different intermolecular interactions and molecular packing patterns, whereas a subtle difference in the distances of the intermolecular interactions could also play a crucial role in the formation of specific polymorphs. Different crystal polymorphs could be interconverted by a simple recrystallization process with a specific solvent, grinding, or fuming. These DHP derivatives had strong intermolecular interactions and/or π–π stacking interactions in their crystal structures, which made it difficult to transform them from a crystalline state to an amorphous state upon grinding. The XRD and DSC experiments revealed that their MC properties could be ascribed to a phase transition between different crystalline states. The reason **TDHP-C$_8$**, **IDHP-C$_n$**, and **NDHP-C$_n$** did not have MC properties might be that they had only one type of crystal and thus could not realize the transformation from one crystalline state to another crystalline state. This work provides new information to for the development of organic fluorescent materials with MC and polymorphic properties.

Acknowledgements

This research work was supported by the National Natural Science Foundation of China (Grants 21572165, 21272176, and 21474048) and the Zhejiang Provincial Natural Science Foundation (Grant LY16B040005).

Notes and references

1 (*a*) J. Mei, Y. Hong, J. W. Y. Lam, A. J. Qin, Y. H. Tang and B. Z. Tang, *Adv. Mater.*, 2014, **26**, 5429–5479; (*b*) Z. G. Chi, X. Q. Zhang, B. J. Xu, X. Zhou, C. P. Ma, Y. Zhang, S. W. Liu and J. R. Xu, *Chem. Soc. Rev.*, 2012, **41**, 3878–3896; (*c*) X. Q. Zhang, Z. G. Chi, Y. Zhang, S. W. Liu and J. R. Xu, *J. Mater. Chem. C*, 2013, **1**, 3376–3390; (*d*) S. P. Anthony, *ChemPlusChem*, 2012, **77**, 518–531; (*e*) S. Varghese and S. Das, *J. Phys. Chem. Lett.*, 2011, **2**, 863–873; (*f*) Y. Sagara and T. Kato, *Nat. Chem.*, 2009, **1**, 605–610; (*g*) H. B. Sun, S. J. Liu, W. P. Lin, K. Y. Zhang, W. Lv, X. Huang, F. W. Huo, H. R. Yang, G. Jenkins, Q. Zhao and W. Huang, *Nat. Commun.*, 2014, **5**, 3601–3609; (*h*) Y. Sagara, S. Yamane, M. Mitani, C. Weder and T. Kato, *Adv. Mater.*, 2016, **28**, 1073–1095.

2 (*a*) H. Y. Zhang, Z. L. Zhang, K. Q. Ye, J. Y. Zhang and Y. Wang, *Adv. Mater.*, 2006, **18**, 2369–2372; (*b*) Y. Zhao, H. Gao, Y. Fan, T. Zhou, Z. Su, Y. Liu and Y. Wang, *Adv. Mater.*, 2009, **21**, 3165–3169; (*c*) K. Wang, H. Zhang, S. Chen, G. Yang, J. Zhang, W. Tian, Z. Su and Y. Wang, *Adv. Mater.*, 2014, **26**, 6168–6173; (*d*) Y. Dong, B. Xu, J. Zhang, X. Tan, L. Wang, J. Chen, H. Lv, S. Wen, B. Li, L. Ye, B. Zou and W. Tian, *Angew. Chem., Int. Ed.*, 2012, **51**, 10782–10785; (*e*) R. Davis, N. P. Rath and S. Das, *Chem. Commun.*, 2004, 74–75; (*f*) C. Li, X. Luo, W. Zhao, C. Li, Z. Liu, Z. Bo, Y. Dong, Y. Q. Dong and B. Z. Tang, *New J. Chem.*, 2013, **37**, 1696–1699; (*g*) R. H. Li, S. Xiao, Y. Li, Q. Lin, R. Zhang, J. Zhao, C. Yang, K. Zou, D. Li and T. Yi, *Chem. Sci.*, 2014, **5**, 3922–3928; (*h*) S. J. Yoon, J. W. Chung, J. Gierschner, K. S. Kim, M. G. Choi, D. Kim and S. Y. Park, *J. Am. Chem. Soc.*, 2010, **132**, 13675–13683; (*i*) K. Nagura, S. Saito, H. Yusa, H. Yamawaki, H. Fujihisa, H. Sato, Y. Shimoikeda and S. Yamaguchi, *J. Am. Chem. Soc.*, 2013, **135**, 10322–10325; (*j*) G. Q. Zhang, J. W. Lu, M. Sabat and C. L. Fraser, *J. Am. Chem. Soc.*, 2010, **132**, 2160–2162; (*k*) E. Sakuda, K. Tsuge, Y. Sasaki and N. Kitamura, *J. Phys. Chem. B*, 2005, **109**, 22326–22331; (*l*) X. Luo, W. Zhao, J. Shi, C. Li, Z. P. Liu, Z. S. Bo, Y. Q. Dong and B. Z. Tang, *J. Phys. Chem. C*, 2012, **116**, 21967–21972; (*m*) Y. Fan, Y. F. Zhao, L. Ye, B. Li, G. Yang and Y. Wang, *Cryst. Growth Des.*, 2009, **9**, 1421–1430; (*n*) X. G. Gu, J. J. Yao, G. X. Zhang, Y. L. Yan, C. Zhang, Q. Peng, Q. Liao, Y. Wu, Z. Z. Xu, Y. S. Zhao, H. B. Fu and D. Q. Zhang, *Adv. Funct. Mater.*, 2012, **22**, 4862–4872; (*o*) L. Chen, S. Y. Yin, M. Pan, K. Wu, H. P. Wang, Y. N. Fan and C. Y. Su, *J. Mater. Chem. C*, 2016, **4**, 6962–6966; (*p*) D. Yan and D. G. Evans, *Mater. Horiz.*, 2014, **1**, 46–57; (*q*) S. Ito, A. Hirose, M. Yamaguchi, K. Tanaka and Y. Chujo, *J. Mater. Chem. C*, 2016, **4**, 5564–5571; (*r*) S. Varughese, *J. Mater. Chem. C*, 2014, **2**, 3499–3516; (*s*) H. Wang, F. Chen, X. Jia, H. Liu, X. Ran, M. K. Ravva, F. Q. Bai, S. Qu, M. Li, H. X. Zhang and J. L. Brédas, *J. Mater. Chem. C*, 2015, **3**, 11681–11688; (*t*) M. J. Percino, M. Cerón, P. Ceballos, G. Soriano-Moro, O. Rodríguez, V. M. Chapela, M. E. Castro, J. Bonilla-Cruz and M. A. Siegler, *CrystEngComm*, 2016, **18**, 7554–7572; (*u*) S. J. Yoon and S. Y. Park, *J. Mater. Chem.*, 2011, **21**, 8338–8346; (*v*) Q. Qi, J. Zhang, B. Xu, B. Li, S. X. A. Zhang and W. Tian, *J. Phys. Chem. C*, 2013, **117**, 24997–25003; (*w*) X. Du, F. Xu, M. S. Yuan, P. Xue, L. Zhao, D. E. Wang, W. Wang, Q. Tu, S. W. Chen and J. Wang, *J. Mater. Chem. C*, 2016, **4**, 8724–8730; (*x*) R. Tan, S. Wang, H. Lan and S. Xiao, *Curr. Org. Chem.*, 2017, **21**, 236–248.

3 (*a*) X. Cheng, H. Zhang, K. Ye, H. Zhang and Y. Wang, *J. Mater. Chem. C*, 2013, **1**, 7507–7512; (*b*) T. Seki, T. Ozaki, T. Okura, K. Asakura, A. Sakon, H. Uekusa and H. Ito, *Chem. Sci.*, 2015, **6**, 2187–2195; (*c*) P. S. Hariharan, D. Moon and

S. P. Anthony, *J. Mater. Chem. C*, 2015, **3**, 8381–8388; (*d*) Y. Zhang, Q. Song, K. Wang, W. Mao, F. Cao, J. Sun, L. Zhan, Y. Lv, Y. Ma, B. Zou and C. Zhang, *J. Mater. Chem. C*, 2015, **3**, 3049–3054; (*e*) O. Toma, N. Mercier and C. Botta, *J. Mater. Chem. C*, 2016, **4**, 5940–5944; (*f*) C. Wang, B. Xu, M. Li, Z. Chi, Y. Xie, Q. Li and Z. Li, *Mater. Horiz.*, 2016, **3**, 220–225; (*g*) Y. X. Li, J. X. Qiu, J. L. Miao, Z. W. Zhang, X. F. Yang and G. X. Sun, *J. Phys. Chem. C*, 2015, **119**, 18602–18610; (*h*) Z. Zhang, Z. Wu, J. Sun, B. Yao, P. Xue and R. Lu, *J. Mater. Chem. C*, 2015, **4**, 2854–2861; (*i*) R. Tan, Q. Lin, Y. Wen, S. Xiao, S. Wang, R. Zhang and T. Yi, *CrystEngComm*, 2015, **17**, 6674–6680; (*j*) Z. He, L. Zhang, J. Mei, T. Zhang, J. W. Y. Lam, Z. Shuai, Y. Q. Dong and B. Z. Tang, *Chem. Mater.*, 2015, **27**, 6601–6607; (*k*) B. Xu, J. He, Y. Mu, Q. Zhu, S. Wu, Y. Wang, Y. Zhang, C. Jin, C. Lo, Z. Chi, A. Lien, S. Liu and J. Xu, *Chem. Sci.*, 2015, **6**, 3236–3241; (*l*) X. Mei, G. Wen, J. Wang, H. Yao, Y. Zhao, Z. Lin and Q. Ling, *J. Mater. Chem. C*, 2015, **3**, 7267–7271; (*m*) Y. Qi, Y. Wang, Y. Yu, Z. Liu, Y. Zhang, G. Du and Y. Qi, *RSC Adv.*, 2016, **6**, 33755–33762; (*n*) C. Botta, S. Benedini, L. Carlucci, A. Forni, D. Marinotto, A. Nitti, D. Pasini, S. Righetto and E. Cariati, *J. Mater. Chem. C*, 2016, **4**, 2979–2989; (*o*) Y. Xu, K. Wang, Y. Zhang, Z. Xie, B. Zou and Y. Ma, *J. Mater. Chem. C*, 2016, **4**, 1257–1262; (*p*) M. Jin, T. Seki and H. Ito, *Chem. Commun.*, 2016, **52**, 8083–8086; (*q*) B. Xu, Y. Mu, Z. Mao, Z. Xie, H. Wu, Y. Zhang, C. Jin, Z. Chi, S. Liu, J. Xu, Y. C. Wu, P. Y. Lu, A. Lien and M. R. Bryce, *Chem. Sci.*, 2016, **7**, 2201–2206; (*r*) P. Galer, R. C. Korošec, M. Vidmar and B. Šket, *J. Am. Chem. Soc.*, 2014, **136**, 7383–7394; (*s*) Y. Wang, G. Zhang, W. Zhang, X. Wang, Y. Wu, T. Liang, X. Hao, H. Fu, Y. Zhao and D. Zhang, *Small*, 2016, **12**, 6554–6561; (*t*) K. Sakurada, T. Seki and H. Ito, *CrystEngComm*, 2016, **18**, 7217–7220; (*u*) M. Li, Q. Zhang, J.-R. Wang and X. Mei, *Chem. Commun.*, 2016, **52**, 11288–11291; (*v*) J. N. Zhang, H. Kang, N. Li, S. M. Zhou, H. M. Sun, S. W. Yin, N. Zhao and B. Z. Tang, *Chem. Sci.*, 2017, **8**, 577–582.

4 Z. Guo, W. Zhu and H. Tian, *Chem. Commun.*, 2012, **48**, 6073–6084.

5 (*a*) C. Shi, Z. Guo, Y. Yan, S. Zhu, Y. Xie, Y. S. Zhao, W. Zhu and H. Tian, *ACS Appl. Mater. Interfaces*, 2013, **5**, 192–198; (*b*) Z. Guo, A. Shao and W. H. Zhu, *J. Mater. Chem. C*, 2016, **4**, 2640–2646.

6 (*a*) H. Tong, M. Häussler, Y. Dong, Z. Li, B. Mi, H. S. Kwok and B. Z. Tang, *J. Chin. Chem. Soc.*, 2006, **53**, 243–246; (*b*) H. Tong, Y. Dong, M. Häussler, Y. Hong, J. Lam, H. Sung, I. D. Williams, H. S. Kwok and B. Z. Tang, *Chem. Phys. Lett.*, 2006, **428**, 326–330; (*c*) H. Tong, Y. Hong, Y. Dong, Y. Ren, M. Häussler, J. W. Y. Lam, K. S. Wong and B. Z. Tang, *J. Phys. Chem. B*, 2007, **111**, 2000–2007; (*d*) H. Li, Y. Guo, G. Li, H. Xiao, Y. Lei, X. Huang, J. Chen, H. Wu, J. Ding and Y. Cheng, *J. Phys. Chem. C*, 2015, **119**, 6737–6748.

7 (*a*) Y. Liu, Y. Lei, F. Li, J. Chen, M. Liu, X. Huang, W. Gao, H. Wu, J. Ding and Y. Cheng, *J. Mater. Chem. C*, 2016, **4**, 2862–2870; (*b*) Y. Lei, Y. Liu, Y. Guo, J. Chen, X. Huang, W. Gao, L. Qian, H. Wu, M. Liu and Y. Cheng, *J. Phys. Chem. C*, 2015, **119**, 23138–23148; (*c*) Y. Liu, Y. Lei, M. Liu, F. Li, H. Xiao, J. Chen, X. Huang, W. Gao, H. Wu and Y. Cheng, *J. Mater. Chem. C*, 2016, **4**, 5970–5980; (*d*) Y. Lei, D. Yang, H. Hua, C. Dai, L. Wang, M. Liu, X. Huang, Y. Guo, Y. Cheng and H. Wu, *Dyes Pigm.*, 2016, **133**, 261–272.

8 (*a*) K. C. Naeem, A. Subhakumari, S. Varughese and V. C. Nair, *J. Mater. Chem. C*, 2015, **3**, 10225–10231; (*b*) C. Niu, Y. You, L. Zhao, D. He, N. Na and J. Ouyang, *Chem. – Eur. J.*, 2015, **21**, 13983–13990.

9 S. Xue, X. Qiu, Q. Sun and W. Yang, *J. Mater. Chem. C*, 2016, **4**, 1568–1578.

10 L. L. Woods, *J. Am. Chem. Soc.*, 1958, **80**, 1440–1442.

11 R. Boonsin, G. Chadeyron, J. P. Roblin, D. Boyer and R. Mahiou, *J. Mater. Chem. C*, 2015, **3**, 9580–9587.

12 G. Kwak, S. Wang, M.-S. Choi, H. Kim, K.-H. Choi, Y.-S. Han, Y. Hur and S.-H. Kim, *Dyes Pigm.*, 2008, **78**, 25–33.

